Nonlinear Behavior in High-Frequency Aggregate Control of Thermostatically Controlled Loads

Ioannis M. Granitsas, Ian A. Hiskens and Johanna L. Mathieu
Department of Electrical Engineering and Computer Science
University of Michigan, Ann Arbor, MI, USA
{igran, hiskens, jlmath}@umich.edu

***Abstract*—Coordinated control of electric loads can provide valuable grid services, such as frequency regulation. However, due to the nonlinear characteristics of such load ensembles, it is important to systematically analyze their behavior and establish a thorough understanding of undesirable phenomena that can potentially arise. In this paper, we analyze the frequency response of an aggregate control scheme, with the goal of exploring controller performance limits. We show that rapid switching commands can induce oscillations in the power output due to the inherent lockout mechanism of the underlying devices. We demonstrate that highly detailed aggregate models are required to capture such phenomena. Such models enable deeper understanding of the control boundaries and therefore play an important role in avoiding the introduction of undesirable effects on the grid.**

***Index Terms*—Demand Response, Frequency Regulation, Thermostatically Controlled Loads, Frequency Response.**

I. Introduction

Control of Thermostatically Controlled Loads (TCLs) such as water heaters, heat pumps or air conditioners (ACs), can provide a variety of services to the grid. However, such load ensembles can exhibit nonlinear behavior and have the potential to induce oscillations in the total power demand. Nonlinear phenomena that arise due to load control have been studied in the past. In the context of electric vehicle charging, hysteresis-based control can exhibit rich dynamical behavior [1]. For TCLs, load synchronization and oscillations have been observed under price-based incentives [2] and set-point control [3]–[5].

As the purpose of TCL aggregate control is to provide some service to power systems, e.g., frequency regulation or renewable tracking, it is important to establish the bandwidth over which such services can be reliably provided. Furthermore, it is important to understand the ways in which aggregate control may fail when pushed beyond its bandwidth, and the consequences of such failure on grid performance. Previous work in the load control literature focuses mainly on assessing performance over a limited regime, thereby offering few insights into controller behaviour under extreme scenarios.

In this paper, we consider the case of relatively high frequency control, e.g., oscillation periods in the range of 30 s to 1800 s, with a controller update rate of 2 s, for the provision of regulation services. We analyze the frequency response of such a control scheme to acquire a deeper understanding of potential undesirable behavior that can arise when the controller is pushed to the extreme. As illustrated in Fig. 1, undesirable oscillations in the power output can be caused by rapid switching commands when the controller tries to follow a reference signal with a 30 s period. These induced oscillations have a much lower dominant frequency, indicated by the solid black line in the figure, compared to the reference signal. As shown in Section IV, these oscillations are directly related to the protective lockout mechanism of the underlying devices. Such lockouts prevent the compressor from turning ON/OFF for some time after each switch to allow sufficient time for the pressure to drop on the high-pressure side of the compressor [6]. We will also explore this behavior through an aggregate model meant to represent the TCL population.

Extensive literature is devoted to developing aggregate models for TCL populations. A common type of aggregate model represents the load ensemble using a Markov transition matrix [7]–[9]. The major benefit of this model class is the low computational effort required to incorporate these models into control applications due to their linearity, which also facilitates a range of state estimation algorithms [10]. There are many variations of such models. Simple versions consider only temperature and compressor ON/OFF mode [10], while more detailed models incorporate more advanced temperature dynamics [11], interactions with the mass temperature [12], [13], multiple zones [14], and lockouts [15]–[19]. The authors of [18], [19] solve an optimization problem to determine a tractable reference signal that will not violate lockout constraints or temperature deadbands. However, this problem assumes prior knowledge of the system operator's balancing signal. Lockouts have also been incorporated using generalized battery models that facilitate flexibility studies [20], [21]. The authors of [21], derive analytical expressions for the reduced power and energy flexibility of the battery model due to lockouts. As will be shown in Section V-A, accurately tracking the progression of TCLs during their lockout phase is required to capture the nonlinearly induced power oscillations. This will be demonstrated by comparing a model that simply accounts for whether a TCL is in lockout [15] with a more detailed model [17] that has an increased number of states to incorporate the time period spent in lockout.

This work was supported by an ARPA-E Open 2018 Award, Number DE-AR0001061.

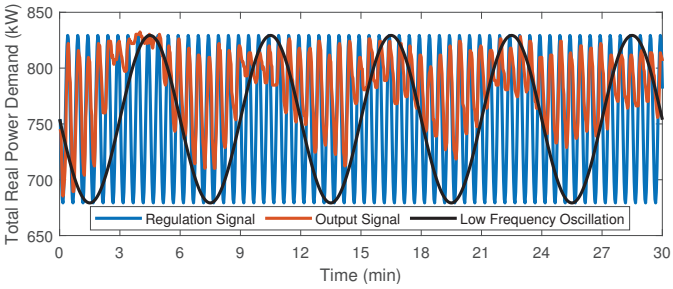

Fig. 1. Power consumption (output) when tracking a sinusoidal reference signal of 30 s period. The controller is not able to follow the reference signal and a low-frequency power oscillation indicated by the solid black line emerges due to lack of availability.

The contributions of this paper are as follows. Firstly, we explore potential nonlinearities of aggregate TCL control over a wide range of frequencies. Secondly, we demonstrate that power oscillations can arise when tracking fast reference signals and show that they are related to the protective lockout mechanism that limits how frequently a TCL can switch. Thirdly, we show that detailed aggregate models are required to capture the observed oscillatory behavior.

The remainder of the paper is organized as follows. Section II describes the operation of individual TCLs, while Section III introduces the controller. The frequency response results when controlling a TCL aggregation are presented in Section IV. Section V shows that highly detailed aggregated models are required to capture the observed oscillations, presents an existing extended aggregate model with lockouts, and explores the differences in the frequency response results when controlling this model versus when controlling the actual population. Section VI concludes the paper.

II. Operation of Individual Devices

The paper considers direct ON/OFF control of residential ACs. ACs configured as ON/OFF TCLs are sometimes called "two-stage" devices. While variable-speed ACs are becoming more common than two-stage devices internationally, in the U.S. in 2011 only 5% of air conditioners were variable speed [22], with projections that this will grow to only 25% by 2055 [23]. This is why we focus on ON/OFF TCLs in this paper.

Each unit is modelled through the 3-state model described in [24], which incorporates both air and mass temperature dynamics, and an ON/OFF mode. Those are governed by,

$$\dot{T}(t) = A_T T(t) + B_T z_T(t), \tag{1}$$

where T includes the air and mass temperatures T_a, T_m of the house, and z_T incorporates the various heat injections, the outdoor temperature and the compressor ON/OFF mode s. The details are omitted for brevity and can be found in [24].

Each AC is equipped with a hysteretic control logic that is responsible for maintaining the indoor air temperature within a deadband around a user-specified set-point. Assuming cooling operation, the compressor turns ON whenever the regulated air temperature exceeds the upper limit of the deadband $T_{\max}$, and OFF whenever it reaches the lower limit $T_{\min}$. This logic is described by,

$$s(t^+) = \begin{cases} s(t)+1, & \text{if } s(t)=0 \ \wedge \ T_a(t) = T_{max} \\ s(t)-1, & \text{if } s(t)=1 \ \wedge \ T_a(t) = T_{min}, \end{cases} \tag{2}$$

where t^+ represents the time instant immediately following the time t at which the regulated air temperature encounters $T_{\max}$ or $T_{\min}$.

AC operation includes a protective mechanism called lockout, meant to protect the equipment by ensuring that the unit does not switch too frequently. More specifically, when the compressor of an AC turns ON or OFF, a time duration of seconds to minutes must elapse before the unit is permitted to switch back to its previous state. This lockout duration is predetermined by the manufacturer and cannot be altered. Consequently, this mechanism imposes a physical constraint on how rapidly and how extensively a collection of TCLs can be controlled. In fact, it gives rise to interesting nonlinear phenomena, as will be demonstrated in subsequent sections.

III. Controller

This section describes the controller used to track the various reference signals associated with providing grid services. This controller achieves satisfactory tracking performance while maintaining relatively low complexity. It is based on representing the TCL population through an aggregate model. Hence, it has the advantage of significantly simplifying computations, making the approach more scalable.

A. Aggregate TCL model

The linear model developed in [10] is able to capture the dominant characteristics of a TCL population with relatively low complexity. The temperature deadband of each device is normalized to a common range and then divided into N_b temperature intervals. Each bin is characterized by its temperature bounds and the compressor ON/OFF mode. Hence, a total number of $2N_b$ bins are used to represent the aggregation. The model is commonly referred to as a "bin model."

This modelling framework facilitates the representation of the TCL population through a Linear Time-Invariant (LTI) model,

$$\begin{aligned} x(k+1) &= Ax(k) + Bu(k), \\ y(k) &= Cx(k), \end{aligned} \tag{3}$$

where $x \in \mathbb{R}^{2N_b \times 1}$ is the state vector that represents the percentage of the population in each bin. Matrix $A \in \mathbb{R}^{2N_b \times 2N_b}$ is the transpose of a Markov Transition Matrix that captures the natural evolution of TCLs. It is formed by the transition probabilities between all states. These probabilities can be computed by counting state transitions during an uncontrolled period prior to controller deployment. It should be noted that the majority of the entries of A are zero, as transitions mainly occur between adjacent bins.

The control input $u(k)$ is designed to switch (or not) the compressor mode of the TCL. The absolute value of each

entry of the control vector represents the fraction of the corresponding bin population that should switch. TCLs are switched either ON or OFF based on whether the entries of u are positive or negative, respectively. Thus, matrix $B \in \mathbb{R}^{2N_b \times N_b}$ redistributes bin contents according to the control vector,

$$B = \begin{bmatrix} \text{diag}(-\mathbf{1}_{N_b}) \\ \text{adiag}(\mathbf{1}_{N_b}) \end{bmatrix}, \tag{4}$$

where functions $\text{diag}(\cdot)$ and $\text{adiag}(\cdot)$ transform their argument into a diagonal and anti-diagonal matrix, respectively, and $\mathbf{1}$ represents a vector of ones with length given by the corresponding subscript.

It should be noted that it is common for bins that correspond to high temperature and ON mode as well as bins that correspond to low temperature and OFF mode to be excluded from control. This avoids switching TCLs that have recently switched, otherwise lockout can lead to temperatures exceeding the limits $[T_{\text{min}}, T_{\text{max}}]$. We refer to bins where controlled switching is not allowed as uncontrolled bins.

Assuming that state measurements are available, the controller receives the portion of the population at each bin, as well as the aggregate power consumption. Therefore, $C \in \mathbb{R}^{(2N_b+1)\times 2N_b}$ has the form:

$$C = \begin{bmatrix} C_p \\ \mathbf{I}_{2N_b} \end{bmatrix}, \tag{5}$$

where $\mathbf{I}$ is the identity matrix and C_p maps x to the aggregate power via the approximation:

$$C_p = \bar{P}_{\text{ON}} N_{\text{TCL}} \begin{bmatrix} \mathbf{0}_{N_b}^{\intercal} & \mathbf{1}_{N_b}^{\intercal} \end{bmatrix}. \tag{6}$$

In (6), $\mathbf{0}$ represents a vector of zeros, N_{TCL} is the total number of TCLs in the population and $\bar{P}_{\text{ON}}$ is the average consumption of TCLs whose compressor is ON. This value is found when constructing the A matrix. Note that if only output feedback is available, a Kalman filter can be used in order to acquire an estimate of the states [10].

B. Controller logic

Control commands are based on a prediction of the aggregate power consumption for the subsequent time instant using the model described in Section III-A. Under uniform control, we require the same number of TCLs to be switched from every bin that is targeted by the controller at each timestep. More specifically, the j^{th} entry of the control vector $u \in \mathbb{R}^{N_b}$ is computed as

$$u^{(j)}(k) = \frac{1}{N_b - N_{\text{unc}}} \frac{K_p \left(P_{\text{ref}}(k+1) - C_p A x(k)\right)}{\bar{P}_{\text{ON}} N_{\text{TCL}}}, \tag{7}$$

where P_{ref} is the reference signal, K_p the controller gain, and N_{unc} is the number of uncontrollable bins. For each uncontrollable bin, the respective entry of u is equal to zero. A derivation of the above control policy is provided in [15].

The vector u_r sent to each TCL is formed by dividing each entry of the control vector u by the associated entry of x in order to convert the input from fractions based on the total number of TCLs to fractions based on the number of TCLs in the corresponding bin. Vector u_r is broadcast to all TCLs. Each device picks the appropriate entry of that vector based on its temperature and ON/OFF state and then determines whether to switch or not. This is decided by drawing a random number, comparing it with the corresponding value of u_r and if it is smaller, the TCL switches. Note that as a result, the actual number of switches will not necessarily be exactly the same as desired. This difference, along with the error associated with the aggregate power prediction for the next timestep, leads to small reference tracking error.

IV. Frequency Response

A. Preliminaries

It is important to characterize the frequency response of a TCL aggregation, and so establish a more complete understanding of behavior across different regimes. Illustrations make use of a population of 1000 individual TCLs operating as described in Section II. A homogeneous population with parameters derived from [24] is considered for simplicity, however the qualitative observations also hold for a heterogeneous population. The outdoor temperature is held constant at 32.2°C and the ON/OFF lockout times are set to 5 min in order to highlight the observed phenomena more clearly, even though a typical lockout value is 3-5 min after turning OFF [6], [25] and 30 sec after turning ON based on our experience. The implications of using these more realistic lockout values are discussed in Section IV. Each simulation has a length of 1 h. The simulation timestep is set to 2 s, matching the time granularity of fast PJM regulation signals [26].

To explore the frequency response of a TCL aggregation, we introduce sinusoidal variation of the controller reference signal and consider a range of frequencies. This process ensures that energy is simply shifted over time rather than increased or decreased during the control event. The total number of cycles within a 1-hour duration was gradually increased resulting in increasingly faster signals with periods ranging from 1800 s to 30 s. All signals were centered around the mean power draw of the unforced TCL population, while the amplitude was a tunable parameter defined as a percentage of the aforementioned mean power draw.

To generate the frequency response curves and also to find the frequency content of the various signals, we used a one-side Fast Fourier Transform (FFT). Before transformation, the mean of the signal was subtracted and a low-pass filter with a cutoff frequency of 0.25 Hz was used as an anti-aliasing mechanism. This ensured that the spectral information extracted from the signal was free from distortions caused by frequencies beyond the Nyquist limit.

B. Frequency response curves

Fig. 2 demonstrates the frequency response curves for different values of input signal amplitudes. Each of these curves was constructed as follows. For every reference signal, the power consumption (output) of the population was decomposed using the approach described in Section IV-A to find the magnitude corresponding to the dominant frequency.

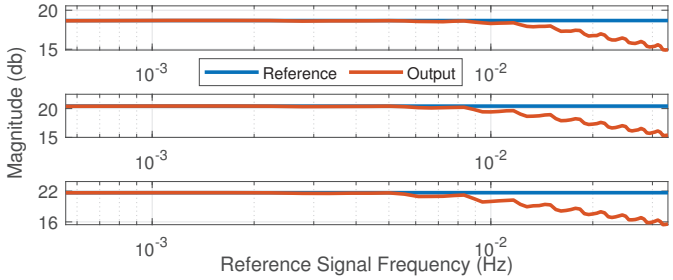

Fig. 2. Frequency response curves for 10% (top), 15% (middle), and 20% (lower) signal amplitudes. As the amplitude of the reference signals increases, the performance degrades.

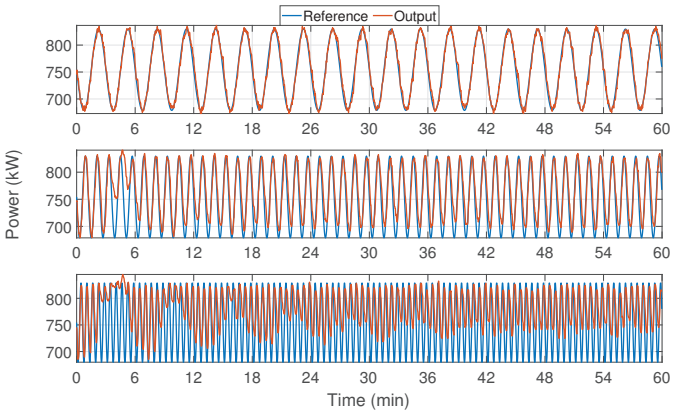

Fig. 3. Power output and reference for slow (top), medium (middle), and high frequency reference signal.

Each of these magnitudes was then plotted in db versus the corresponding reference signal frequency. Greater deviation from the flat blue horizontal line indicates worse tracking performance.

It can be observed that as the amplitude of the reference signal increases, the frequency at which performance starts to deteriorate decreases. This is expected due to the reduced availability of the TCL population, which results from an increasing proportion of devices being uncontrollable due to lockouts.

Interestingly, when performance starts to degrade, low frequency oscillations arise in the power output. These extraneous oscillations are referred to as low frequency since they are much slower compared to the primary frequency of the power output and the reference signal. The oscillations become more and more evident as the reference frequency increases. This can be observed in the outputs shown in Fig. 3 for three different reference signals. In the top plot, there is no loss of availability and tracking is very accurate for the slowly varying reference signal. For the intermediate frequency shown in the middle plot, notice the start of clipping in the lower parts of the power consumption. That clipping effect evolves into the low frequency oscillation in the bottom plot as the reference signal frequency is further increased.

The underlying reason for these oscillations is the significant number of lockouts caused by the intrusive control actions required to match the rapid reference signal. Fig. 4 shows power output that exhibits the aforementioned clipping along with the corresponding percentage of the population that

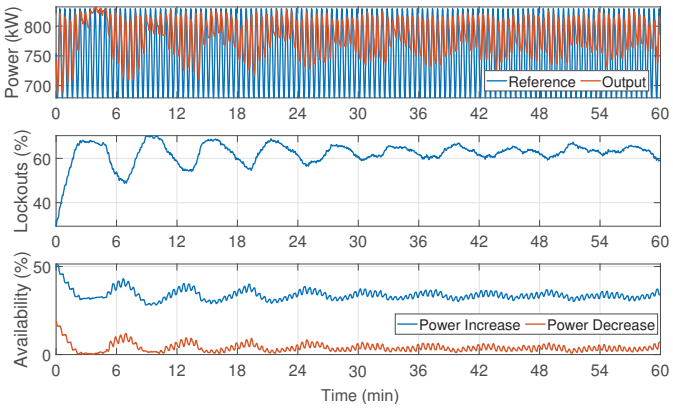

Fig. 4. Power output (top), locked percentage (middle), and control availability (bottom) for a high-frequency input signal with a period of 30 s.

is locked and the power available for up/down adjustment. Starting from an uncontrolled state, additional control effort is required to initiate tracking of the reference signal, thereby leading to quick depletion of available power due to TCLs becoming locked. From that point onward, the controller is attempting to match the lower sections of the reference signal, using nearly all available capacity for power decrease. The available downward adjustment capability exhibits an oscillation that has a much lower frequency compared to the reference signal. This happens because the groups of TCLs that were controlled during the initial phase become available after their lockouts end, only to be switched again and forced into a new lockout phase. Hence, the slower oscillation in the power output matches the frequency of the locked percentage and the availability. It should be noted that this illustration is driven by depleted availability for power decrease. However, a similar phenomenon can be observed for power increase under different conditions and parameters.

The above observation holds beyond the individual case discussed. To demonstrate, Fig. 5 shows the dominant low frequency of the power output and the dominant frequency of the locked percentage for the wide spectrum of sinusoidal inputs that were tested. Since the dominant frequency of the power output always matches the reference frequency, we find the dominant low frequency by searching below 80% of the reference frequency for the frequency with the next highest spectral density. We are interested in the reference frequency range for which performance is not satisfactory (above 10 mHz). Over that range, it can be observed that the dominant low frequency of the output power approximately matches the frequency of the locked percentage.

It should be noted that the results and observations of this section still hold qualitatively for different lockout duration values. In the perhaps more realistic scenario in which lockouts are on the order of 3 min and 30 s after turning OFF and ON respectively, we found that the aggregate power still exhibited oscillatory behavior. Due to the smaller lockout times, oscillations became evident for higher reference signal amplitudes. Also, because lockouts were not symmetric after turning ON or OFF, the dominant frequencies of the locked percentages

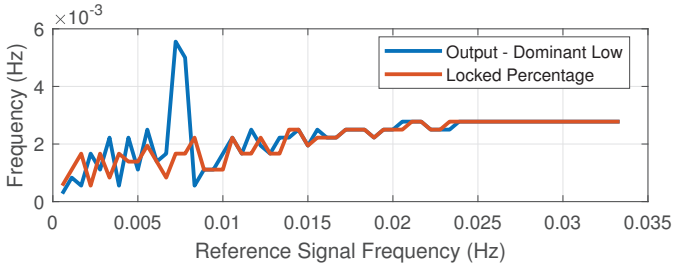

Fig. 5. Dominant low frequency of the power output and dominant frequency of the locked percentage for different reference signal frequencies.

varied more, relative to the dominant low frequency of the power, than was the case in Fig. 5.

C. Impact of heterogeneity

The results in Section IV-B were for a homogeneous population. However, the aforementioned qualitative observations also hold for the heterogeneous case. To show that, we form a heterogeneous aggregation that consists of TCLs with thermal parameters drawn from uniform distributions around $\pm 20\%$ of their nominal values.

The main observation of Section IV-B was that due to lockouts, the available power adjustment oscillated, causing an oscillation with very similar frequency in the power output. When using the heterogeneous population, the frequency of the output power oscillation is still close to the frequency of the availability oscillation. However, the oscillations evolve differently between the two population types. We used a Short-Time Fourier Transform (STFT) to visualize this difference. Fig. 6 depicts the dominant low frequency of the power output of the two population types when tracking a fast sinusoidal signal with a period of 30 s. It can be seen that the low-frequency oscillation degrades faster in the heterogeneous case compared to the homogeneous case. This happens because TCLs progress at different rates in the temperature domain due to different thermal parameters and some of the TCLs that became locked at the early tracking stages are not within controllable bins after the lockouts end. Moreover, focusing on the latter half of the simulations shown in Fig. 6, even though the oscillation is not as prevalent as in the beginning, there is still a nonzero signal power. For the heterogeneous case, this is spread out in more frequencies compared to the homogeneous case for the same reason that caused faster degradation of the oscillation. It should be noted that the impact of heterogeneity on the oscillations is similar to other sources of randomness, such as disturbances from user activities.

D. Mitigation of oscillations

One way of limiting the oscillations, and also verifying their underlying cause described in Section IV-B, is to limit the control effort during the initial phase of the control event. This can be achieved using a soft-starter mechanism when initiating control. Such an approach adjusts the controller gain to prevent a large amount of TCLs from becoming locked at similar times. Note that even though performance will be degraded initially by using that mechanism, the impact

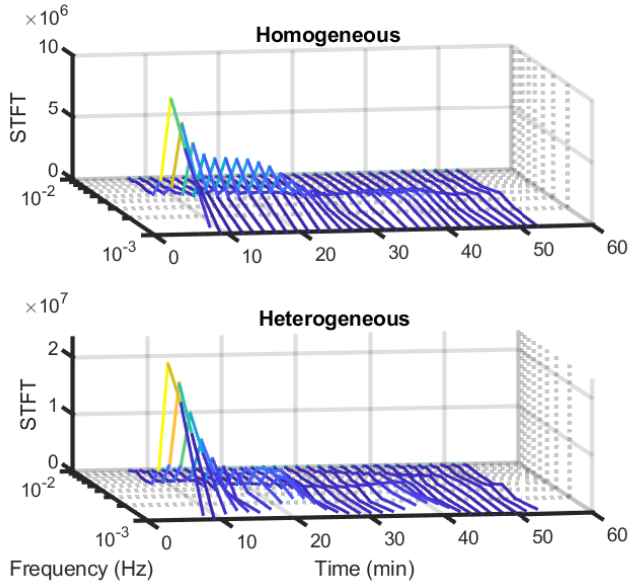

Fig. 6. Comparison of the dominant low frequency of the power output for a homogeneous versus a heterogeneous population. The oscillation degrades faster for the heterogeneous population.

on overall tracking may be small because oscillations are mitigated.

Given a nominal controller gain K_p, a simple implementation of the soft-starter idea would be to consider a linear gain scheduler,

$$\tilde{K}_p(t) = \min(K_p, \alpha t + \tilde{K}_p^0), \tag{8}$$

where the slope α is computed based on the desired initial controller gain $\tilde{K}_p^0$ and the desired time τ_s that the soft starter should be disabled. Both of these are design parameters. As a result, the slope is given by,

$$\alpha = \frac{K_p - \tilde{K}_p^0}{\tau_s}. \tag{9}$$

The resulting adjusted gain $\tilde{K}_p(k)$ is therefore used in (7) instead of K_p to compute the fraction of devices to switch. After time τ_s has elapsed, the controller gain remains fixed at the nominal value K_p.

An example of the effect of the soft-starter, with $\tilde{K}_p^0 = 0.1$ and $\tau_s = 800$ s, is illustrated in Fig. 7. Notice that the power oscillations observed during the initial phase of the top plot (corresponding to the case without a soft-starter) are mitigated in the middle plot due to the control modification. This happens because the gain reduction of the soft-starter prevents the controller from forcing a significant number of TCLs into the lockout state. As a result, the oscillation in lockout percentage that is observed without a soft-starter is mitigated, as illustrated in the bottom plot of Fig. 7. This also verifies the intuition regarding the cause of power oscillations.

Also note that even though the controller is not utilized to its full extent during the initial phase of the control event, the overall tracking performance is not degraded. The Normalized Root Mean Squared (NRMS) error for the soft-starter case is 6.55% compared to 6.83% without.

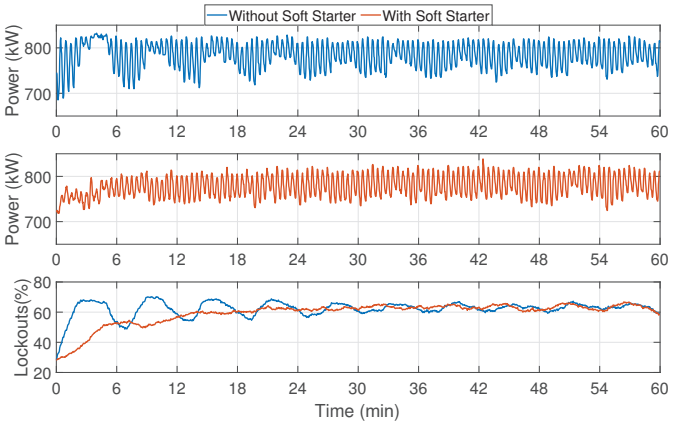

Fig. 7. Power output without (top) and with (middle) using a soft starter, along with the corresponding percentages of locked TCLs (bottom) for a high-frequency input signal with a period of 30 s. The low frequency oscillation during the initial phase of the control event is mitigated by the soft stater.

V. Extended Aggregate State Space Model

A. Formulation

It is appealing to consider an aggregate model of the TCL population that is able to capture the rich dynamical behavior observed in Section IV. Such a model offers an opportunity to reproduce and analyze the population dynamics without needing to separately model every individual device. The proposed abstraction represents the system using a Markov Transition Matrix as in Section III-A, but with extended states that enable accurate tracking of lockouts across the population, an essential step towards capturing the observed oscillations. The proposed model is similar to that of [17].

This revised model, referred to as an extended bin model with lockouts, again builds on an LTI form (3). In the bin model described in Section III-A, henceforth referred to as the basic bin model, the state vector is comprised of $2N_b$ states that encapsulate all temperature bins for the two modes of operation (ON/OFF). The extended bin model with lockouts includes one such vector for every possible number of timesteps remaining until the lockout ends.

The state vector of the extended bin model with lockouts is constructed by concatenating the states corresponding to the unlocked TCLs x_0, followed by the states corresponding to the locked TCLs x_l for $l = 1, ..., T_L$, where l is the number of timesteps until the lockout ends and T_L is the maximum number of timesteps until the lockout ends. We order the vectors x_l from highest to lowest remaining time until lockout ends. Hence, the state vector $x \in \mathbb{R}^{2N_b(T_L+1)\times 1}$ is defined as,

$$x = \begin{bmatrix} x_0^\intercal & x_{T_L}^\intercal & x_{T_L-1}^\intercal & \dots & x_2^\intercal & x_1^\intercal \end{bmatrix}^\intercal. \tag{10}$$

Each vector $x_l \in \mathbb{R}^{2N_b\times 1}$ includes the states corresponding to l remaining timesteps until lockout ends and is defined as,

$$x_l = \begin{bmatrix} x_{l,1}^{\text{OFF}} & x_{l,2}^{\text{OFF}} & \dots & x_{t_l,N_b}^{\text{OFF}} & x_{l,N_b}^{\text{ON}} & x_{l,N_b-1}^{\text{ON}} & \dots & x_{l,1}^{\text{ON}} \end{bmatrix}^\intercal. \tag{11}$$

The state $x_{l,b}^s$ is determined by three factors: the temperature bin b, the compressor ON/OFF mode s, and the remaining lockout timesteps l. Bins are defined in increasing temperature order for the OFF states and in decreasing order for the ON states. For simplicity of presentation, we assume that the lockout duration is the same regardless of whether the TCL switches ON or OFF. However, the approach extends to the case with different ON and OFF lockout durations.

For the unlocked states, bin transitions are similar to those in the basic model. However, for the locked states, transitions include both a deterministic and a probabilistic aspect. Temperature evolves probabilistically based on the transition probabilities of the basic model, while the remaining lockout timesteps are reduced deterministically by one after each iteration. Hence, all content of the bins corresponding to a certain remaining lockout value l will move to the bins corresponding to the remaining lockout value $l-1$, taking into account the probabilities that govern transitions between temperature intervals and ON/OFF modes in the basic bin model.

The transition matrix A for the extended bin model with lockouts uses the transition matrix of the basic bin model. Specifically, it uses the same probabilities for transitioning between temperature intervals, with the only difference being that when TCLs switch, they move to the states x_{T_L} corresponding to maximum remaining lockout. Moreover, for all bins associated with locked states, the probability of remaining in those bins is zero, as the remaining lockout time is constantly decreasing.

The control vector $u \in \mathbb{R}^{2N_b\times 1}$, which is directed to only the unlocked states, has entries that give the desired switch probability for each bin. Its action is to move devices from the states x_0 to the states x_{T_L}. Since TCLs are switched either ON or OFF at every time instant, one half of the control vector is always zero. Matrix $B \in \mathbb{R}^{2N_b(T_L+1)\times 2N_b}$ ensures proper movement of TCLs between the bins,

$$B = \begin{bmatrix} -\mathbf{I}_{N_b} & \mathbf{0}_{N_b} \\ \mathbf{0}_{N_b} & -\mathbf{I}_{N_b} \\ \mathbf{0}_{N_b} & \mathbf{J}_{N_b} \\ \mathbf{J}_{N_b} & \mathbf{0}_{N_b} \\ \mathbf{0}_{2N_b(T_L-1)} & \mathbf{0}_{2N_b(T_L-1)} \end{bmatrix}, \tag{12}$$

where $\mathbf{J}$ is a square matrix with ones in the anti-diagonal and zeros everywhere else. For the case of full-state feedback, matrix $C \in \mathbb{R}^{(2N_b(T_L+1)+1)\times 2N_b(T_L+1)}$ is defined as,

$$C = \begin{bmatrix} \mathbf{I}_{2N_b(T_L+1)} \\ C_p \end{bmatrix}, \tag{13}$$

where $C_p \in \mathbb{R}^{1\times 2N_b(T_L+1)}$ is,

$$C_p = N_{\text{TCL}}\bar{P}_{\text{ON}} \begin{bmatrix} \mathbf{0}_{1\times N_b} & \mathbf{1}_{1\times N_b} \dots \mathbf{0}_{1\times N_b} & \mathbf{1}_{1\times N_b} \end{bmatrix}. \tag{14}$$

B. Comparison with existing models

The model presented in Section V-A precisely describes the evolution over time of the locked portion of the TCL population. This is a vital step in creating an aggregate model that captures the observed oscillations, since they are directly related to the lockouts, as discussed in Section IV-B. In contrast, the model is not well suited for control applications due to its high dimensionality.

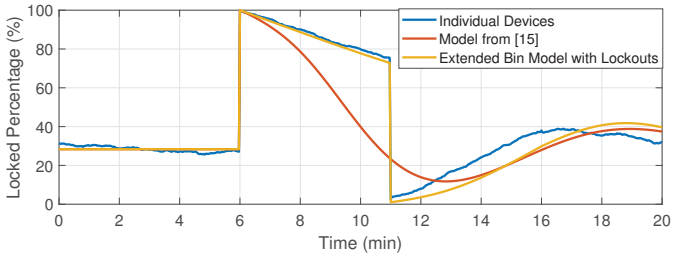

Fig. 8. Comparison of the lockout percentage between a collection of individual devices, the bin model from [15], and the extended bin model with lockouts. All available TCLs are switched at 6 min. The extended bin model with lockouts is better able to capture the changes in locked percentage following the initial switch.

Previously developed models are not able to achieve the accuracy required for investigating nonlinear phenomena induced by lockouts. The widely used model described in Section III-A ignores lockouts. The direct extension of that model doubled the length of the state vector by considering a bin for the locked part of every existing bin [15].

To demonstrate why this is not sufficient, Fig. 8 shows the lockout responses of the extended bin model with lockouts and the model presented in [15], and provides a comparison with the collective response of many individual device models. The two bin models have very similar steady-state behavior, which approximately matches that of the collection of individual devices. After an initial idle period where the population was in steady state, all available devices were switched at 6 min. Beyond that time, the responses of the two bin models differ considerably.

Intuitively, simultaneous switching of a large group of TCLs should result in a spike in the lockouts. This should be followed by a slow decrease in lockouts as devices that were already locked become unlocked. Eventually the lockout percentage will suddenly drop as the large group of switched TCLs complete their lockout period. This form of behavior is indeed displayed by the collection of individual devices shown in blue, and is closely matched by the response of the extended bin model with lockouts shown in yellow. In contrast, the model developed in [15] fails to capture the sudden spike of availability occurring after the switched TCLs complete their lockout period. This is a consequence of the model [15] not explicitly capturing TCL temperature variation during the lockout phase. Rather, it only considers whether TCLs are locked or not, resulting in a constant rate of devices becoming unlocked. This rate becomes inaccurate during control action, however, as it is based on the unforced population and is therefore a result of its natural switching rate.

C. Frequency response of the extended bin model

The same frequency sweep conducted in Section IV-B can be carried out using the extended bin model with lockouts. This entails using the same controller logic as described in Section III-B on the bin model described in Section V-A with $N_b = 20$. Fig. 9 compares the resulting frequency response curve with that obtained by controlling the individual devices. Outdoor temperature is considered constant at 32.2°C and the

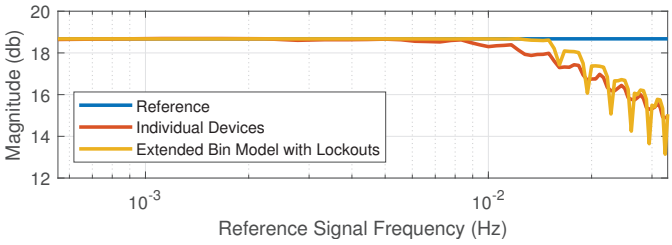

Fig. 9. Frequency response comparison between controlling the individual devices and controlling the extended bin model with lockouts.

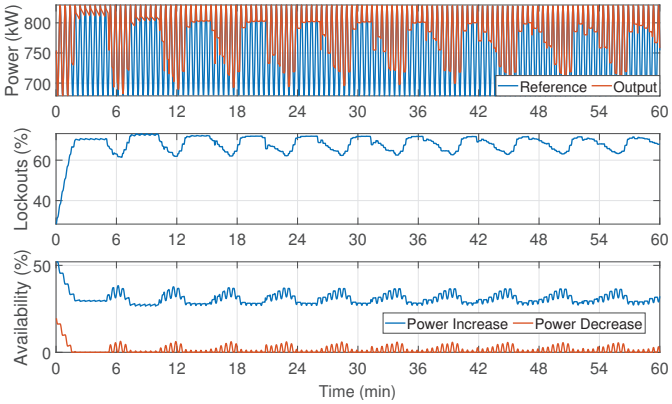

Fig. 10. Power output (top), locked percentage (middle), and control availability (bottom) for a high-frequency input signal with a period of 30 s when controlling the extending bin model with lockouts.

ON/OFF lockout periods are set at 5 min. The regulation signal amplitude is set to 10% of the mean power draw of the uncontrolled TCL population. We observe that controlling the bin model rather than the actual population results in a higher critical frequency. This is due to the absence of noise in switching. That noise results from the probabilistic nature of the controller that causes the actual number of switches to deviate slightly from the desired value, as well as in the prediction error resulting from the transition matrix A.

Fig. 10 shows an example of the output when controlling the extended bin model with lockouts to track a fast sinusoidal input. It can be observed that the emergent oscillations are indeed captured by the model and display similar frequency as in Fig. 4. It should be noted that the outputs between the two cases differ because of switching error/noise that is not present when controlling the extended bin model with lockouts. This explains why oscillations persist in the extended bin model output, rather than displaying some damping as in Fig. 4.

The extended bin model with lockouts closely tracks the reference signal for lower reference frequencies and no extraneous oscillations are evident. As the reference frequency increases, however, a low frequency oscillation emerges. Fig. 11 shows that over the relevant higher-frequency range, the extended bin model with lockouts accurately predicts the low frequency oscillations that occurs in the power output and the locked percentage.

VI. Conclusions

The paper explores nonlinear phenomena that can arise when an aggregation of TCLs is controlled to track a high

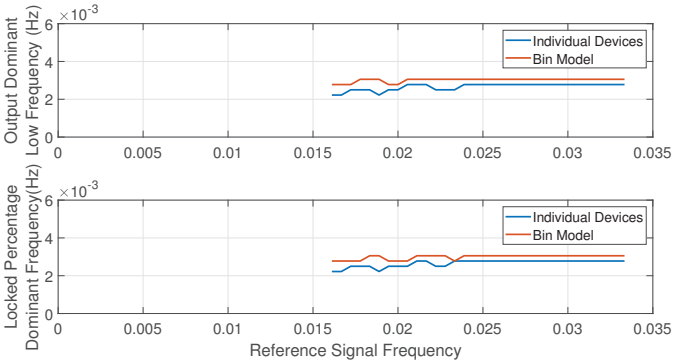

Fig. 11. Comparison of the emergent oscillation frequency for the output power (top) and the locked percentage (bottom), for a collection of individual devices and the extended bin model with lockouts.

frequency reference signal. The frequency response of such an aggregation was analyzed to gain a better understanding of controller behavior across different regimes. It was shown that tracking high frequency sinusoidal reference signals can cause low frequency oscillations in the power output due to synchronization of TCLs in the lockout phase. Note that such clear oscillatory behavior may not be evident in practice as real dispatch signals are unlikely to include such high frequency components together with significant power densities. However, the impact of reduced availability that is periodically depleted could still be observed. Moreover, it was shown that aggregate models which explicitly incorporate TCL temperature variation during the lockout phase are capable of capturing the observed oscillations.

Future work includes exploring the effects that TCL-induced power oscillations may have on the grid. Moreover, even though the frequency response characterization through sinusoidal excitation is standard for linear systems, our results show clearly that the system is nonlinear, and hence motivate the need for more appropriate characterization. For that reason, we will also undertake systematic limit cycle analysis to more precisely quantify the factors underpinning the emergence of low-frequency oscillations.

REFERENCES

[1] S. Kundu and I. A. Hiskens, "Nonlinear dynamics of hysteresis-based load controls," *IFAC Proceedings Volumes*, vol. 47, no. 3, pp. 5419–5425, 2014, 19th IFAC World Congress.

[2] M. S. Nazir and I. A. Hiskens, "A dynamical systems approach to modeling and analysis of transactive energy coordination," *IEEE Trans Power Systems*, vol. 34, no. 5, pp. 4060–4070, 2019.

[3] N. Mahdavi, J. H. Braslavsky, and C. Perfumo, "Mapping the effect of ambient temperature on the power demand of populations of air conditioners," *IEEE Trans Smart Grid*, vol. 9, no. 3, pp. 1540–1550, 2018.

[4] C. Perfumo, J. Braslavsky, J. K. Ward, and E. Kofman, "An analytical characterisation of cold-load pickup oscillations in thermostatically controlled loads," in *Australian Control Conference*, 2013, pp. 195–200.

[5] W. Bomela, A. Zlotnik, and J.-S. Li, "A phase model approach for thermostatically controlled load demand response," *Applied Energy*, vol. 228, pp. 667–680, 2018.

[6] R. T. Ruminsky, "Compressor minimum off-time system," US Patent 4,128,854, December 5, 1978.

[7] L. C. Totu, R. Wisniewski, and J. Leth, "Demand response of a TCL population using switching-rate actuation," *IEEE Trans Control Systems Technology*, vol. 25, no. 5, pp. 1537–1551, 2017.

[8] S. Bashash and H. K. Fathy, "Modeling and control of aggregate air conditioning loads for robust renewable power management," *IEEE Trans Control Systems Technology*, vol. 21, no. 4, pp. 1318–1327, 2013.

[9] D. S. Callaway, "Tapping the energy storage potential in electric loads to deliver load following and regulation, with application to wind energy," *Energy Conversion and Management*, vol. 50, no. 5, pp. 1389–1400, 2009.

[10] J. L. Mathieu, S. Koch, and D. S. Callaway, "State estimation and control of electric loads to manage real-time energy imbalance," *IEEE Trans Power Systems*, vol. 28, no. 1, pp. 430–440, 2013.

[11] I. M. Granitsas, I. A. Hiskens, and J. L. Mathieu, "Incorporating delayed temperature dynamics into residential air conditioner models for grid frequency regulation," in *IEEE Conference on Control Technology and Applications*, 2022, pp. 439–446.

[12] W. Zhang, J. Lian, C.-Y. Chang, and K. Kalsi, "Aggregated modeling and control of air conditioning loads for demand response," *IEEE Trans on Power Systems*, vol. 28, no. 4, pp. 4655–4664, 2013.

[13] M. Liu and Y. Shi, "Model predictive control of aggregated heterogeneous second-order thermostatically controlled loads for ancillary services," *IEEE Trans Power Systems*, vol. 31, no. 3, pp. 1963–1971, 2016.

[14] S. A. Nugroho, I. M. Granitsas, J. L. Mathieu, and I. A. Hiskens, "Aggregate modeling and non-disruptive control of residential air conditioning systems with two-zone cooling capacity," in *American Control Conference*, 2022, pp. 4668–4675.

[15] S. Ross and J. Mathieu, "Strategies for network-safe load control with a third-party aggregator and a distribution operator," *IEEE Trans Power Systems*, vol. 36, no. 4, pp. 3329–3339, 2021.

[16] C.-Y. Chang, W. Zhang, J. Lian, and K. Kalsi, "Modeling and control of aggregated air conditioning loads under realistic conditions," in *IEEE PES Innovative Smart Grid Technologies Conference*, 2013, pp. 1–6.

[17] M. Liu and Y. Shi, "Optimal control of aggregated heterogeneous thermostatically controlled loads for regulation services," in *IEEE Conference on Decision and Control*, 2015, pp. 5871–5876.

[18] A. Coffman, A. Bušić, and P. Barooah, "A unified framework for coordination of thermostatically controlled loads," *Automatica*, vol. 152, p. 111002, 2023.

[19] A. R. Coffman, N. Cammardella, P. Barooah, and S. Meyn, "Aggregate flexibility capacity of TCLs with cycling constraints," *IEEE Trans on Power Systems*, vol. 38, no. 1, pp. 52–62, 2023.

[20] ——, "Flexibility capacity of thermostatically controlled loads with cycling/lock-out constraints," in *American Control Conference*, 2020, pp. 527–532.

[21] C. Ziras, S. You, H. W. Bindner, and E. Vrettos, "A new method for handling lockout constraints on controlled tcl aggregations," in *Power Systems Computation Conference*, 2018, pp. 1–7.

[22] DOE IEDO. Variable-speed, low-cost motor for residential HVAC systems. Accessed: 2024-03-12. [Online]. Available: https://www.energy.gov/eere/iedo/variable-speed-low-cost-motor-residential-hvac-systems

[23] US Federal Register. Energy conservation program: Energy conservation standards for room air conditioners. Accessed: 2024-03-12. [Online]. Available: https://www.federalregister.gov/documents/2023/05/26/2023-10287/energy-conservation-program-energy-conservation-standards-for-room-air-conditioners

[24] GridLAB-D residential module user's guide. [Online]. Available: http://gridlab-d.shoutwiki.com/wiki/Residential_module_user%27s_guide

[25] *Air Conditioner LW5016 Owner's Manual*, LG Electronics, 2017. [Online]. Available: https://www.lg.com/us/support/product/lg-LW5016.ASWAHDP

[26] PJM ancillary services. [Online]. Available: https://www.pjm.com/markets-and-operations/ancillary-services.aspx